

1 **Seasonal temperature variation influences climate suitability for dengue,**
2 **chikungunya, and Zika transmission**

3 John H. Huber^{1,2}, Marissa L. Childs³, Jamie M. Caldwell², Erin A. Mordecai^{2*}

4

5 ¹Department of Applied and Computational Mathematics and Statistics, University
6 of Notre Dame, Notre Dame, Indiana, USA

7 ²Department of Biology, Stanford University, Stanford, California, USA

8 ³Emmett Interdisciplinary Program in Environment and Resources, Stanford
9 University, Stanford, California, USA

10

11 *Corresponding Author: emordeca@stanford.edu

12

13 Short title: Seasonal climate affects vector transmission

14 **Abstract**

15 Dengue, chikungunya, and Zika virus epidemics transmitted by *Aedes aegypti*
16 mosquitoes have recently (re)emerged and spread throughout the Americas,
17 Southeast Asia, the Pacific Islands, and elsewhere. Understanding how
18 environmental conditions affect epidemic dynamics is critical for predicting and
19 responding to the geographic and seasonal spread of disease. Specifically, we lack a
20 mechanistic understanding of how seasonal variation in temperature affects
21 epidemic magnitude and duration. Here, we develop a dynamic disease
22 transmission model for dengue virus and *Aedes aegypti* mosquitoes that integrates
23 mechanistic, empirically parameterized, and independently validated mosquito and
24 virus trait thermal responses under seasonally varying temperatures. We examine
25 the influence of seasonal temperature mean, variation, and temperature at the start
26 of the epidemic on disease dynamics. We find that at both constant and seasonally
27 varying temperatures, warmer temperatures at the start of epidemics promote
28 more rapid epidemics due to faster burnout of the susceptible population. By
29 contrast, intermediate temperatures (24-25°C) at epidemic onset produced the
30 largest epidemics in both constant and seasonally varying temperature regimes.
31 When seasonal temperature variation was low, 25-35°C annual average
32 temperatures produced the largest epidemics, but this range shifted to cooler
33 temperatures as seasonal temperature variation increased (analogous to previous
34 results for diurnal temperature variation). Tropical and sub-tropical cities such as
35 Rio de Janeiro, Fortaleza, and Salvador, Brazil; Cali, Cartagena, and Barranquilla,
36 Colombia; Delhi, India; Guangzhou, China; and Manila, Philippines have mean annual

37 temperatures and seasonal temperature ranges that produced the largest
38 epidemics. However, more temperate cities like Shanghai, China had high epidemic
39 suitability because large seasonal variation offset moderate annual average
40 temperatures. By accounting for seasonal variation in temperature, the model
41 provides a baseline for mechanistically understanding environmental suitability for
42 virus transmission by *Aedes aegypti*. Overlaying the impact of human activities and
43 socioeconomic factors onto this mechanistic temperature-dependent framework is
44 critical for understanding likelihood and magnitude of outbreaks.

45

46 **Non-Technical Summary (150-200 Words)**

47 Mosquito-borne viruses like dengue, Zika, and chikungunya have recently caused
48 large epidemics that are partly driven by temperature. Using a mathematical model
49 built from laboratory experimental data for *Aedes aegypti* mosquitoes and dengue
50 virus, we examine the impact of variation in seasonal temperature regimes on
51 epidemic size and duration. At constant temperatures, both low and high
52 temperatures (20°C and 35°C) produce small epidemics, while intermediate
53 temperatures like 25°C and 30°C produce much larger epidemics. In seasonally
54 varying temperature environments, epidemics peak more rapidly at higher starting
55 temperatures, while intermediate starting temperatures produce the largest
56 epidemics. Seasonal mean temperatures of 25-35°C are most suitable for large
57 epidemics when seasonality is low, but in more variable seasonal environments
58 epidemic suitability peaks at lower annual average temperatures. Tropical and sub-
59 tropical cities have the highest temperature suitability for epidemics, but more

60 temperate cities with high seasonal variation also have the potential for very large
61 epidemics.

62 **Introduction**

63 Over the last 30-40 years, arboviral outbreaks have dominated the public health
64 landscape globally [1]. These viruses, most notably dengue (DENV), chikungunya
65 (CHIKV), and Zika (ZIKV), can cause symptoms ranging from rash, arthralgia, and
66 fever to hemorrhagic fever (DENV), long-term arthritis (CHIKV), Guillain-Barré
67 syndrome and microcephaly (ZIKV) [2–4]. DENV, which historically spread
68 worldwide along shipping routes [5], places 3.97 billion individuals at risk
69 worldwide [6] and causes an estimated 390 million cases annually, including 96
70 million symptomatic cases [7]. CHIKV was introduced into the Americas in
71 December 2013 after an outbreak in St. Martin Island [8]. Since then, autochthonous
72 transmission has been reported in 45 countries [9], and 1.3 billion people
73 worldwide are at risk of contracting CHIKV [10]. More recently, the ZIKV epidemic
74 in the Americas captured global attention after the World Health Organization
75 (WHO) designated it a Public Health Emergency of International Concern in
76 February 2016 in response to its association with neurological disorders. Following
77 the first reported case in Brazil in May 2015, ZIKV has spread to 48 countries and
78 territories where it is transmitted autochthonously [11]. Because DENV, CHIKV, and
79 ZIKV are mostly transmitted by *Aedes aegypti* mosquitoes, they may have similar
80 geographic distributions and risk factors.

81 Informed public health decisions to limit the spread and magnitude of these
82 arboviral epidemics depend on a robust understanding of transmission dynamics.
83 One mechanistic modeling framework, the Susceptible – Infected – Recovered (SIR)
84 model, has been implemented successfully to model the dynamics of outbreaks of

85 influenza, measles, and vector-borne diseases such as CHIKV and ZIKV [12–14]. This
86 approach tracks virus population dynamics by compartmentalizing individuals by
87 their state in an epidemic (i.e., Susceptible (S), Infected (I), Recovered (R)). This
88 framework can be extended to include additional compartments, such as a latency
89 stage, or to incorporate the dynamics of the mosquito population for vector
90 transmission.

91 Arbovirus dynamics are strikingly seasonal and geographically restricted to
92 relatively warm climates [6,7]. This arises because several life history traits of the
93 mosquitoes that transmit DENV, CHIKV, and ZIKV are strongly influenced by
94 temperature and seasonality [15–22]. For simplicity, many existing models assume
95 static life history traits [14], and those that address seasonal forcing tend to
96 incorporate sinusoidal variation as a single transmission parameter, β [23]. Treating
97 seasonal temperature variation as a sinusoidal forcing function on the transmission
98 parameter implies a monotonic relationship between temperature and
99 transmission, such that transmission is maximized at high temperatures and
100 decreases at low temperatures. However, decades of experimental work have
101 demonstrated strongly nonlinear (often unimodal) relationships between mosquito
102 and pathogen traits and temperature that are not well captured in a single
103 sinusoidal forcing function [24]. Efforts by Yang et al. [25,26] addressed the need to
104 include seasonal variation by adopting an SEI-SEIR compartmental framework with
105 time-varying entomological parameters and fitting the model to DENV incidence
106 data in Campinas, Brazil. Other previous work has integrated the effects of
107 temperature on mosquito and parasite traits into temperature-dependent

108 transmission models for DENV, CHIKV, and/or ZIKV, and revealing a strong,
109 nonlinear influence of temperature with peak transmission between 29 – 35 °C [27–
110 34]. However, we do not yet have a mechanistic estimate for the relationship
111 between seasonal temperature regimes and transmission potential, incorporating
112 the full suite of transmission-relevant, nonlinear thermal responses of mosquito and
113 parasite traits.

114 Here, we expand on previous work with three main advances: (1) we
115 incorporate the full suite of empirically-derived, unimodal thermal responses for all
116 known transmission-relevant mosquito and parasite traits; (2) we examine the
117 influence of seasonal temperature mean and variation (in contrast to constant
118 temperatures or daily temperature variation); and (3) we use a dynamic
119 transmission framework to explore the impact of different seasonal temperature
120 regimes on the epidemiologically-relevant outcomes of epidemic size, duration, and
121 peak incidence (in contrast to R_0 , or vectorial capacity, which are difficult to
122 measure directly). To do so, we incorporate previously estimated and independently
123 validated thermal response functions for all vector and parasite traits [24] into a
124 dynamic SEI-SEIR model [25,26]. We explore field-relevant temperature regimes by
125 simulating epidemics across temperature means (10 – 38°C) and seasonal ranges (0
126 – 17°C) from across the predicted suitable range for transmission. Specifically, we
127 use the model to ask: (1) How does final epidemic size vary across constant
128 temperatures? (2) Under seasonally varying temperatures, how does the
129 temperature at the start of the epidemic affect the final epidemic size and duration?
130 (3) How do temperature mean and seasonal range interact to determine epidemic

131 size? (4) Which geographic locations have high epidemic suitability based on
132 climate?

133

134 **Methods**

135 **Model**

136 Model Framework

137 We adopted an SEI-SEIR compartmental modeling framework to simulate arboviral
138 transmission by the *Aedes aegypti* vector (Fig. 1). We introduced temperature-
139 dependence into the model by using fitted thermal response curves for the
140 mosquito life history traits provided by Mordecai et al. [24]. The full model is:

141

$$142 \quad \frac{dS_V}{dt} = EFD(T) * pEA(T) * MDR(T) * \mu(T)^{-1} * N_V * \left(1 - \frac{N_V}{K(T)}\right) - \left(a(T) * pMI(T) * \frac{I_H}{N_H} + \mu(T)\right) * S_V, \quad (1)$$

143

$$144 \quad \frac{dE_V}{dt} = a(T) * pMI(T) * \frac{I_H}{N_H} * S_V - (PDR(T) + \mu(T)) * E_V, \quad (2)$$

145

$$146 \quad \frac{dI_V}{dt} = PDR(T) * E_V - \mu(T) * I_V, \quad (3)$$

147

$$148 \quad \frac{dS_H}{dt} = -a(T) * b(T) * \frac{I_V}{N_H} * S_H, \quad (4)$$

149

$$150 \quad \frac{dE_H}{dt} = a(T) * b(T) * \frac{I_V}{N_H} * S_H - \delta * E_H, \quad (5)$$

151

$$152 \quad \frac{dI_H}{dt} = \delta * E_H - \eta * I_H, \quad (6)$$

153

$$154 \quad \frac{dR_H}{dt} = \eta * I_H, \quad (7)$$

155

156 **Fig 1. Compartmental model of transmission.** S_H , E_H , I_H , and R_H represent the
157 susceptible, exposed (or latent), infectious, and recovered segments of the human
158 population, respectively. Likewise, S_V , E_V , and I_V represent the susceptible, exposed
159 (or latent), and infectious segments of the mosquito population. Solid arrows signify
160 the directionality of transition from one compartment to the next, and dashed
161 arrows indicate the directionality of transmission.

162

163 The SEI portion of the model describes the vector population, where S_V
164 represents the number of susceptible mosquitoes, E_V is the number of mosquitoes in
165 the latency stage, and I_V is the number of infectious mosquitoes. We assumed that
166 *Aedes aegypti* mosquitoes remain infectious until they die. In equations 1-3, (T)
167 indicates temperature-dependent functions, $EFD(T)$ is the number of eggs laid per
168 female per day, $pEA(T)$ is the probability of mosquito egg-to-adult survival, $MDR(T)$
169 is the mosquito egg-to-adult development rate, N_V is the total mosquito population
170 at time t (i.e., $S_V + E_V + I_V$), $K(T)$ is the carrying capacity for the mosquito population,
171 $a(T)$ is the per mosquito biting rate, $pMI(T)$ is the probability of mosquito infection
172 per bite on an infectious host, $\mu(T)$ is the adult mosquito mortality rate, and $PDR(T)$
173 is the parasite development rate. Each life history and pathogen transmission trait
174 of the *Aedes aegypti* mosquito is a unimodal, temperature-dependent function fit
175 from experimental laboratory data in previous work [15–22,24] (Table 1; Appendix;
176 “Functional Forms of Life History Traits”).

177

178 **Table 1.** Fitted thermal responses for *Aedes aegypti* life history traits. Traits were fit
 179 to a Brière $[cT(T - T_0)(T_m - T)^{\frac{1}{2}}]$ or a quadratic $[c(T - T_m)(T - T_0)]$ function where
 180 T represents temperature. T_0 and T_m are the critical thermal minimum and
 181 maximum, respectively, and c is the rate constant. Thermal responses were fit by
 182 [24].

Trait	Definition	Function	Fitted Parameters		
a	Biting rate (day ⁻¹)	Brière	$c = 2.02\text{e-}04$	$T_{min} = 13.35$	$T_{max} = 40.08$
EFD	Eggs laid per female per day	Brière	$c = 8.56\text{e-}03$	$T_{min} = 14.58$	$T_{max} = 34.61$
pEA	Probability of mosquito egg-to-adult survival	Quadratic	$c = -5.99\text{e-}03$	$T_{min} = 13.56$	$T_{max} = 38.29$
MDR	Mosquito egg-to-adult development rate (day ⁻¹)	Brière	$c = 7.86\text{e-}05$	$T_{min} = 11.36$	$T_{max} = 39.17$
lf	Adult mosquito lifespan (days)	Quadratic	$c = -1.48\text{e-}01$	$T_{min} = 9.16$	$T_{max} = 37.73$
b	Probability of mosquito infectiousness	Brière	$c = 8.49\text{e-}04$	$T_{min} = 17.05$	$T_{max} = 35.83$
pMI	Probability of mosquito infection	Brière	$c = 4.91\text{e-}04$	$T_{min} = 12.22$	$T_{max} = 37.46$
PDR	Virus extrinsic incubation rate (day ⁻¹)	Brière	$c = 6.65\text{e-}05$	$T_{min} = 10.68$	$T_{max} = 45.90$

183

184

185 The SEIR portion of the model describes the human population, where S_H
 186 represents the number of susceptible individuals, E_H the number of latent (or
 187 exposed) individuals, I_H the number of infectious individuals, and R_H the number of
 188 recovered individuals. We assumed a static population size, N_H , that was neither
 189 subject to births nor deaths because the human lifespan far exceeds the duration of

190 an epidemic. Further, we binned asymptomatic and symptomatic individuals into a
 191 single infectious class since asymptomatic infections have been shown to transmit
 192 DENV [35] and exhibit similar viremic profiles as symptomatic patients in CHIKV
 193 [36]. Based on previous arboviral outbreaks [37,38], we assumed that an infection
 194 conferred long-term immunity to an individual. Thus, a previously infectious
 195 individual entering the recovered class is protected from subsequent re-infection
 196 for the remainder of the epidemic. In the case of dengue, where there are four
 197 unique serotypes, we consider single-season epidemics of a single serotype. In
 198 equations 4-7, $b(T)$ is the probability of human infection per bite by an infectious
 199 mosquito (Table 1), δ^{-1} is the intrinsic incubation period, and η^{-1} is the human
 200 infectivity period. Since human components of the transmission cycle are not
 201 seasonal, we used constants of 5.9 days for the intrinsic incubation period, $1/\delta$, and
 202 5.0 days for the infectious period, $1/\eta$ [14]. All temperature-independent parameter
 203 values are given in Table 2.

204

205 **Table 2.** Values of temperature-independent parameters used in the model, and
 206 their sources.

Parameter	Definition	Value	Source
δ^{-1}	Intrinsic incubation period (days)	5.9	[14]
η^{-1}	Human infectivity period (days)	5.0	[14]
I_0^H/N	Proportion of initially infectious humans	0.0001	
I_0^V/M	Proportion of initially infectious mosquitoes	0.015	[14]

M/N Ratio of mosquitoes-to-humans at 29°C 2.0 [39]

207

208

209 Since the lifespan of an adult mosquito is short relative to the timespan of an

210 epidemic, we allowed mosquito birth and death rates to drive population dynamics.

211 Additionally, the birth rate of susceptible mosquitoes was regulated by a

212 temperature-dependent carrying capacity, K (equation 8), which we modeled as a

213 modified Arrhenius equation that is a unimodal function of temperature [40]:

214

215
$$K(T) = \frac{EFD(T_0) * pEA(T_0) * MDR(T_0) * \mu(T_0)^{-1} - \mu(T_0)}{EFD(T_0) * pEA(T_0) * MDR(T_0) * \mu(T_0)^{-1}} * N_m * e^{\frac{-E_A * (T - T_0)^2}{\kappa_B * (T + 273) * (T_0 + 273)}}, \quad (8)$$

216

217 Here, T_0 is defined as the reference temperature (i.e., the temperature at

218 which the carrying capacity is greatest) in Celsius, N_m is the maximum carrying

219 capacity, and κ_B is Boltzmann constant (8.617×10^{-5} eV/K). EFD is the number of

220 eggs laid per female per day, pEA is the probability of egg-to-adult mosquito

221 survival, MDR is the mosquito egg-to-adult development rate, and μ is the adult

222 mosquito mortality rate. We calculated these values for the reference temperature.

223 E_A is the activation energy, which we set to 0.5 and represents the temperature

224 dependence of the carrying capacity, a conservative estimate as we lacked sufficient

225 data on estimates of the carrying capacity of *Aedes aegypti* and its underlying

226 temperature dependence. To convert from Celsius to Kelvin, we incremented the

227 temperature T and the reference temperature T_0 by 273. Equation (8) was adopted

228 from [40] and modified to allow the distribution to be unimodal. We set the

229 reference temperature, T_0 , to 29°C, which is consistent with optimal temperatures
230 for *Aedes aegypti* transmission [24,29].

231 We included a temperature-dependent carrying capacity in the model to
232 constrain the growth of the mosquito population. As described in the Appendix, all
233 simulations begin with the mosquito population at its (temperature-dependent)
234 carrying capacity. As the temperature changes seasonally, the mosquito population
235 does not necessarily remain at carrying capacity if one or more of the life history
236 traits that determine the production of new mosquitoes in equation (1)— EFD , pEA ,
237 and MDR —is equal to zero. This occurs below 14.58°C (the highest T_{min} of EFD , pEA ,
238 and MDR) or above 34.61°C (the lowest T_{max} of EFD , pEA , and MDR).

239 It should be noted that the transmission parameters are only related to the
240 current temperature at each time point in the simulation. Time lags for each life
241 history trait were not explicitly built into the model.

242

243 Seasonal Forcing

244 To address seasonality in the model, we allowed temperature to vary over
245 time. We modeled temperature as a sinusoidal curve with a period of 365 days of
246 the form:

247

$$248 \quad T(t) = \frac{T_{max} - T_{min}}{2} * \sin\left(\frac{2\pi}{365}t\right) + T_{mean}, \quad (9)$$

249

250 Here, T_{max} , T_{mean} , and T_{min} represent the average monthly maximum, mean, and
251 minimum temperatures across a calendar year, respectively, and t is measured in

252 days. By modeling temperature as a function of time, we allowed the life history
253 traits of the *Aedes aegypti* vector to vary across time for the duration of the
254 epidemic. In the absence of a specific focal location we modeled seasonal
255 temperature as a sinusoidal function for simplicity.

256

257 **Data**

258 Life History Traits

259 To incorporate seasonal forcing into the compartmental modeling framework, we
260 used fitted mechanistic thermal response curves [24]. Mordecai et al. [24] examined
261 published data on thermal responses for life history traits of the *Aedes aegypti*
262 vector and DENV and adopted a Bayesian approach for fitting quadratic ($Q(T)$; Eq.
263 10) or Brière ($B(T)$; Eq. 11) curves (see Appendix for details).

264

$$265 \quad Q(T) = c * (T - T_{min}) * (T - T_{max}), \quad (10)$$

266

$$267 \quad B(T) = c * T * (T - T_{min}) * \sqrt{T_{max} - T}, \quad (11)$$

268

269 Here, c is a rate constant, T_{min} is the critical temperature minimum, and T_{max} is the
270 critical temperature maximum (Table 1). Following Mordecai et al. [24], we
271 assumed values above the critical thermal maxima and below the minima were
272 equal to zero.

273 Mordecai et al. [24] fit the thermal response for adult mosquito lifespan
274 (Table 1), the inverse of the adult mosquito mortality rate (μ , in days⁻¹), used in our

275 model. We set the mortality rate at temperatures outside the critical thermal
276 minimum and maximum to 24 days^{-1} (i.e., mosquitoes survive for one hour at
277 temperatures outside of the T_{\min} to T_{\max} range).

278

279 Historical Weather Data

280 To identify areas of epidemic suitability across the globe, we extracted
281 monthly mean temperatures for 2016 from Weather Underground
282 (wunderground.com) for twenty different cities (Table 3). For each city, we
283 calculated the mean, minimum, and maximum from the average monthly mean
284 temperatures, to estimate temperature seasonality. This provided a range of the
285 average monthly temperature over the span of a calendar year. We chose this time
286 period because it provided the most recent full calendar year to demonstrate
287 seasonal variation in temperature.

288

289 **Table 3.** Temperature regimes for major cities during the 2016 calendar year.

290 Monthly mean temperatures during 2016 were extracted from Weather
291 Underground.

292

City	Annual Mean Temperature (°C)	Annual Temperature Amplitude (°C)
Buenos Aires, Argentina	16.5	8.0
Sao Paulo, Brazil	20.6	5.0

Rio de Janeiro, Brazil	24.3	4.0
Salvador, Brazil	26.3	2.0
Fortaleza, Brazil	27.8	0.50
Belo Horizonte, Brazil	21.9	3.0
Recife, Brazil	27.2	1.5
Shanghai, China	17.6	12.5
Beijing, China	12.8	16
Guangzhou, China	22.9	8.0
Bogotá, Colombia	14.7	1.0
Medellin, Colombia	17.9	1.0
Cali, Colombia	25.1	1.5
Barranquilla, Colombia	28.8	1.0
Cartagena, Colombia	28.6	1.0
Delhi, India	26.3	9.5
Tokyo, Japan	17.0	10.5
Kobe, Japan	17.4	11
Manila, Philippines	29.0	1.5
New York, USA	13.8	12

293

294

295 **Variability in Epidemic Dynamics with Constant Temperature**

296 We first examined how epidemic dynamics varied across different constant

297 temperatures. Here, we did not introduce seasonal forcing into the model but rather

298 assumed static life history traits for *Aedes aegypti* for the simulation period. We
299 simulated the model under default starting conditions (see Appendix) at four
300 different constant temperatures: 20°C, 25°C, 30°C, and 35°C. These temperatures
301 were chosen to span the range of temperatures at which arbovirus transmission is
302 likely to be possible [24].

303

304 **Variability in Epidemic Dynamics with Starting Temperature**

305 Using the model that included seasonal variation in temperature, we examined how
306 the dynamics of an epidemic varied due to the temperature at which the epidemic
307 began, under two temperature regimes. First, we set $T_{max} = 40.0^{\circ}\text{C}$, $T_{mean} = 25.0^{\circ}\text{C}$,
308 and $T_{min} = 10.0^{\circ}\text{C}$ in the time-varying seasonal temperature model under default
309 parameters (see Appendix) and varied the temperature at the start of the epidemic
310 from 10.0°C to 40.0°C in increments of 0.1°C. We examined the response of final
311 epidemic size, epidemic length, and maximum instantaneous number of infected
312 individuals. We then repeated this process for a regime with a lower magnitude of
313 seasonal temperature variation: $T_{max} = 30.0^{\circ}\text{C}$, $T_{mean} = 25.0^{\circ}\text{C}$, and $T_{min} = 20.0^{\circ}\text{C}$. By
314 comparing these temperature regimes, we can examine how epidemics respond to
315 starting temperatures that are outside the range of plausible temperatures of
316 arbovirus transmission (regime 1) versus restricted to the plausible temperatures
317 for transmission (regime 2) [24].

318

319 **Seasonal Variability of Final Epidemic Size**

320 Using the compartmental modeling framework with the default starting conditions,
321 we examined the variation in final epidemic size as a result of seasonal forcing. To
322 do so, we simulated over a wide range of temperature mean and seasonal variance
323 regimes. The mean annual temperature varied from 10.0°C to 38.0°C in increments
324 of 0.1°C, while the seasonal variation about the mean (i.e., $\frac{T_{max}-T_{min}}{2}$) ranged from
325 0.0°C to 17.0°C in increments of 0.1°C. Many of these temperature regimes are
326 unlikely to be observed empirically. However, the simulated temperature regimes
327 spanned the full range of feasible temperature conditions. We recorded the final
328 epidemic size, measured as the number of individuals in the recovered
329 compartment at the end of the simulation, for each unique combination of mean
330 annual temperature and seasonal variation. In addition, we examined the effect of
331 epidemic starting temperature on final epidemic size across the same seasonal
332 temperature regimes. We ran the model under default starting conditions, but
333 allowed the starting temperature to equal T_{min} , T_{mean} , or T_{max} .

334 To observe the interaction of population immunity with the seasonal
335 temperature regime, we simulated the model assuming that 0, 20, 40, 60, or 80% of
336 the population was initially immune. Each simulation began with the introduction
337 of the infected individual occurring at the mean seasonal temperature.

338 We then compared simulated climate regimes with actual climates in major
339 cities, to measure relative epidemic suitability of the following cities: São Paulo,
340 Brazil; Rio de Janeiro, Brazil; Salvador, Brazil; Fortaleza, Brazil; Belo Horizonte,
341 Brazil; Recife, Brazil; Bogotá, Colombia; Medellín, Colombia; Cali, Colombia;
342 Barranquilla, Colombia; Cartagena, Colombia; Tokyo, Japan; Delhi, India; Manila,

343 Philippines; Shanghai, China; Beijing, China; New York City, USA; Guangzhou, China;
344 Kobe, Japan; and Buenos Aires, Argentina, given 0, 20, 40, 60, and 80% population
345 immunity. These cities were chosen because they represent some of the most
346 populous urban areas across South America and throughout the world.

347

348 **Model Sensitivity and Uncertainty Analysis**

349 To characterize uncertainty in the model, we sampled 50 joint posterior estimates
350 for c , T_{min} , and T_{max} for each life history trait provided by Mordecai et al. [24]. We
351 examined the variability in epidemic dynamics with starting temperatures under
352 each parameterization and report the 95% credible interval for the epidemiological
353 indices. We similarly characterize uncertainty in our estimates of the final epidemic
354 size as a function of the seasonal temperature regime by simulating under each
355 parameterization and reporting the 95% credible interval.

356

357 **Results**

358 **Variability in Epidemic Dynamics with Constant Temperature**

359 Holding temperature constant, we examined variability in epidemic dynamics
360 across four temperatures: 20°C, 25°C, 30°C, and 35°C. As temperature increased
361 from 20°C to 30°C, the number of susceptible individuals depleted more rapidly
362 (Fig. 2, S_H). At 20°C and 35°C, the epidemics were small (1.33% and 5.92% of the
363 population infected, respectively) and burned out rapidly. Although simulations run
364 at 25°C and 30°C produced final epidemic sizes of 94.73% and 99.98% of the

365 population infected, respectively (Fig. 2, R_H), the epidemic peaked much faster at
366 30°C.

367

368 **Fig 2. Variation in epidemic dynamics by temperature.** The model was simulated
369 under default parameters at four constant temperatures: 20°C, 25°C, 30°C, and 35°C.

370

371 **Variability in Epidemic Dynamics with Starting Temperature**

372 Next, we examined variability in epidemic dynamics due to the temperature at
373 which the epidemic began, given two seasonal temperature regimes (25°C mean and
374 a seasonal range of 10°C to 40°C or 20°C to 30°C, respectively). Given that an
375 epidemic occurred, epidemic length monotonically decreased as a function of
376 starting temperature for the first temperature regime (Fig. 3, A): warmer
377 temperatures at the start of the epidemic produced shorter epidemics, and vice
378 versa. In the second temperature regime, epidemic length monotonically decreased
379 as a function of starting temperature until ~29°C. When temperature varied from
380 10°C to 40°C, the longest epidemic simulated was 137.8 days and occurred at
381 starting temperatures of 11.2°C, and the shortest epidemic lasted 16.82 days and
382 occurred when the temperature at the epidemic start was 35.7°C. When the
383 temperature was 35.8°C or higher or 10.2°C or lower, no epidemic occurred. When
384 temperature was constrained between 20°C and 30°C, the longest epidemic
385 simulated was 253.64 days at a starting temperature of 20°C, and the shortest
386 epidemic lasted 136.1 days at a starting temperature of 28.9°C.

387

388 **Fig 3. Epidemiological indices as a function of starting temperature, within a**
389 **given seasonal temperature regime.** The red curve represents the maximum
390 number of humans in the infected class (I_H) at any given point during the simulation.
391 The blue curve represents the final (or cumulative) epidemic size (R_H at the final
392 time step). The green curve represents the length of the epidemic (i.e., the point at
393 which the number of infected individuals was below one). Here, simulations were
394 run with the temperature conditions: $T_{min} = 10^\circ\text{C}$, $T_{mean} = 25^\circ\text{C}$, and $T_{max} = 40^\circ\text{C}$ (A)
395 and $T_{min} = 20^\circ\text{C}$, $T_{mean} = 25^\circ\text{C}$, and $T_{max} = 30^\circ\text{C}$ (B).

396

397 In contrast to epidemic length, the response of final epidemic size and
398 maximum number of infected individuals to the temperature at epidemic onset
399 depended on the amount of seasonal temperature variation. When temperature
400 varied widely, from 10°C to 40°C , both final epidemic size and the maximum
401 number of infected individuals responded unimodally to starting temperature, with
402 peaks at 23.9°C and 24.1°C , respectively (Fig. 3, A). By contrast, when temperature
403 varied more narrowly from 20°C to 30°C , the final epidemic size and the maximum
404 number of infected individuals were insensitive to starting temperature (Fig. 3, B).
405 Taken together, these results show that epidemics introduced at different times
406 within identical seasonal temperature regimes can produce very similar final
407 epidemic sizes and maximum infection rates, provided that the temperature range is
408 sufficiently constrained. If temperature variation is large, dramatically different final
409 epidemic sizes and maximum infection rates may result.

410

411 **Seasonal Variability of Final Epidemic Size**

412 To address how mean temperature and seasonal variance combined to influence the
413 final epidemic size, we simulated over a wide range of temperature regimes that
414 accounted for variation in the mean and temperature range over a calendar year.
415 We calculated relative epidemic suitability, defined as the final epidemic size as a
416 proportion of the human population, for twenty major cities worldwide (Table 3).

417 In a low-variation thermal environment, a band of mean temperatures
418 between approximately 25°C and 35°C supports the highest epidemic suitability
419 (Fig. 4). As the seasonal temperature range increases, lower mean temperatures are
420 capable of supporting large epidemics. However, outside this narrow band of
421 temperature regimes, epidemic suitability rapidly diminishes, and most
422 temperature regimes did not produce epidemics.

423

424 **Table 3.** Estimates of epidemic suitability for major cities. Epidemic suitability was
425 calculated as the proportion of the population that became infected in simulations
426 run with 0, 20, 40, 60, or 80% initial population immunity. Temperature at
427 simulation onset was set to the mean of the temperature regime. Each city was
428 simulated with its respective temperature regime from the 2016 calendar year.

429

Epidemic Suitability

City	0% Immunity	20% Immunity	40% Immunity	60% Immunity	80% Immunity
------	-------------	--------------	--------------	--------------	--------------

Buenos Aires, Argentina	0.03656	0.02169	0.01203	0.005975	0.002295
Sao Paulo, Brazil	0.6056	0.3386	0.1518	0.05351	0.01385
Rio de Janeiro, Brazil	0.9984	0.7962	0.5891	0.3618	0.09862
Salvador, Brazil	0.9990	0.7976	0.5937	0.3804	0.1335
Fortaleza, Brazil	0.9993	0.7982	0.5953	0.3861	0.1535
Belo Horizonte, Brazil	0.5909	0.3344	0.1544	0.05771	0.01633
Recife, Brazil	0.9994	0.7985	0.5959	0.3871	0.1517
Shanghai, China	0.9966	0.7878	0.5507	0.2484	0.03456
Beijing, China	0.5268	0.2526	0.09058	0.02298	0.003587
Guangzhou, China	0.9996	0.7989	0.5965	0.3848	0.1254

Bogotá,	0.0001000	0.0001000	0.0001000	0.0001000	0.0001000
Colombia					
Medellin,	0.002544	0.002048	0.001556	0.001068	0.0005820
Colombia					
Cali,	0.9909	0.7822	0.5617	0.3122	0.07217
Colombia					
Barranquilla,	0.9997	0.7993	0.5979	0.3928	0.1703
Colombia					
Cartagena,	0.9997	0.7993	0.5978	0.3923	0.1688
Colombia					
Delhi, India	0.9537	0.7215	0.4759	0.2388	0.06803
Tokyo, Japan	0.7269	0.4149	0.1758	0.05159	0.009489
Kobe, Japan	0.9435	0.6669	0.3522	0.1090	0.01632
Manila,	0.9998	0.7994	0.5981	0.3933	0.1720
Philippines					
New York,	0.04088	0.02159	0.01041	0.004390	0.001425
USA					

430

431 **Table 4. Estimates of epidemic suitability for major cities under different**

432 **starting temperatures.** Epidemic suitability was calculated as the proportion of the

433 population that became infected in simulations that began at the minimum, mean, or

434 maximum temperature of the seasonal temperature regime. Each city was simulated

435 with its respective temperature regime from the 2016 calendar year with 0%

436 population immunity.

437

Epidemic Suitability

City	Minimum Starting Temperature	Mean Starting Temperature	Maximum Starting Temperature
Buenos Aires, Argentina	0.0001000	0.03656	0.1166
Sao Paulo, Brazil	0.02026	0.6056	0.3480
Rio de Janeiro, Brazil	0.9978	0.9984	0.9760
Salvador, Brazil	0.9965	0.9990	0.9963
Fortaleza, Brazil	0.9986	0.9993	0.9990
Belo Horizonte, Brazil	0.09404	0.5909	0.3273
Recife, Brazil	0.9973	0.9994	0.9987
Shanghai, China	0.0001000	0.9966	0.8905
Beijing, China	0.0001000	0.5268	0.5792
Guangzhou, China	0.9983	0.9996	0.9912
Bogotá, Colombia	0.0001000	0.0001000	0.0001000
Medellin, Colombia	0.0002177	0.002544	0.004472
Cali, Colombia	0.9858	0.9909	0.9623
Barranquilla, Colombia	0.9994	0.9997	0.9997
Cartagena, Colombia	0.9993	0.9997	0.9997
Delhi, India	0.5615	0.9537	0.6954

Tokyo, Japan	0.0001000	0.7269	0.5121
Kobe, Japan	0.0001000	0.9435	0.6890
Manila, Philippines	0.9994	0.9998	0.9998
New York, USA	0.0001000	0.04088	0.1863

438

439 **Fig 4. Variation in epidemic suitability across different seasonal temperature**

440 **regimes.** The heat map shows the epidemic suitability (represented as the
441 proportion of the total human population infected during an epidemic) as a function
442 of mean annual temperature and temperature range. Here, temperature range is
443 defined as the seasonal variation about the annual mean temperature. Twenty large,
444 globally important cities are plotted to illustrate their epidemic suitability.

445

446 Of the focal 20 major cities, those with high mean temperature and small
447 average temperature variation exhibited the highest epidemic suitability. For
448 instance, Manila, Philippines, which has a monthly mean temperature of 29°C and
449 average seasonal amplitude in mean temperature of 1.50°C, had an epidemic
450 suitability of 0.9998. Cartagena and Barranquilla, Colombia had epidemic suitability
451 of 0.9997. On the other hand, areas with low average temperature and greater
452 temperature variation, such as Beijing and New York, exhibited lower—but still
453 non-zero—epidemic suitabilities of 0.5268 and 0.04088 respectively. Notably,
454 Guangzhou and Shanghai, China have high epidemic suitability (0.9996 and 0.9966,
455 respectively) despite moderate mean temperatures (22.9 and 17.6°C, respectively)
456 due to high seasonal variation in temperature. By contrast, high seasonal variation

457 reduced suitability to 0.9537 in Delhi, India, which has a high mean temperature of
458 26.3°C (Fig. 4).

459 The relationship between epidemic suitability and seasonal temperature
460 regime was consistent across varying levels of population immunity. Locations with
461 high mean temperatures and small average temperature variation had higher
462 epidemic suitability, regardless of the level of population immunity (Figures S2-S5).
463 However, as the level of immunity increased from 20% to 80%, the epidemic
464 suitability at given seasonal temperature regime decreased (Table 3).

465 Epidemic suitability also varied by starting temperature, depending on the
466 seasonal temperature regime. The epidemic suitability of cities with high mean
467 temperature and small average temperature variation—such as Manila, Philippines
468 and Cartagena and Barranquilla, Colombia—did not depend on starting temperature
469 (Table 4). However, areas with low to moderate mean temperature and large
470 average temperature variation (e.g., Kobe, Japan and Shanghai, China) exhibited low
471 epidemic suitability (both 0.0001000) at the minimum starting temperature and
472 moderate-to-high epidemic suitability at the maximum starting temperature
473 (0.6890 and 0.8905, respectively) (Fig. 5). The opposite occurred in regimes with
474 high mean temperature and large temperature variation, though these temperature
475 regimes are rarer.

476 Estimated epidemic suitability is close to one in the most suitable
477 temperature regimes because we assumed that: (i) the population was fully
478 susceptible at the start of the epidemic; (ii) mixing was homogeneous among
479 humans and mosquitoes; (iii) all cases of infection are included regardless of

480 whether or not they are symptomatic; and (iv) no other environmental or social
481 drivers are limiting transmission. As a result, the epidemic suitability metric should
482 be considered an upper bound on the proportion of the population that could
483 become infected based on temperature alone.

484

485 **Fig 5. Variation in epidemic suitability across different seasonal temperature**

486 **regimes averaged across starting temperatures.** The heat map shows the
487 epidemic suitability (represented as the proportion of the total human population
488 infected during an epidemic) as a function of mean annual temperature and
489 temperature range averaged across simulations where the initial temperature was
490 set to the seasonal temperature regime's minimum, mean, or maximum
491 temperature. Here, temperature range is defined as the seasonal variation about the
492 annual mean temperature. Twenty large, globally important cities are plotted to
493 illustrate their epidemic suitability.

494

495 **Model Sensitivity and Uncertainty Analysis**

496 Final epidemic size was not sensitive to life history trait parameterization (Figs. S8-
497 S10), using samples from the posterior distribution of thermal response fits for each
498 temperature-dependent trait.

499 There was uncertainty in the specific numerical values of the epidemiological
500 indices across starting temperatures (Fig. S1). However, the overall functional
501 response of the final epidemic size, maximum number of infected individuals, and

502 the epidemic length to starting temperature was consistent across the samples from
503 the joint posterior distribution.

504

505 **Discussion**

506 Recent outbreaks of DENV, CHIKV, and ZIKV in Latin America and across the
507 globe have captured the attention of the public health community and underscore
508 the importance of preparation for future outbreaks. As temperatures rise, the global
509 landscape suitable for such outbreaks will expand and shift geographically,
510 potentially placing a larger proportion of the world's population at risk [24,29,31].
511 Understanding how local temperature regimes govern epidemic dynamics is
512 increasingly important for determining resource allocation and control
513 interventions [41]. While previous work has investigated the effects of temperature
514 on DENV, CHIKV, and/or ZIKV transmission, until now we have lacked
515 comprehensive, mechanistic, and dynamic understanding of the effects of seasonally
516 varying temperature on transmission via its (nonlinear) effects on mosquito and
517 parasite traits [27–34]. With our model, which expands on [24] and [25], we show
518 that seasonal temperature mean and amplitude interact with the temperature at
519 epidemic onset to shape the speed and magnitude of epidemics.

520 At constant temperature, epidemics varied substantially in the rate at which
521 susceptible individuals were depleted. Epidemics simulated at 25°C and 30°C
522 reached similar sizes but the epidemic at 25°C proceeded at a much slower rate (Fig.
523 2). This “slow burn” phenomenon occurs because slower depletion of susceptible
524 individuals can produce epidemics of similar size to epidemics that infect people

525 very rapidly. This phenomenon also occurs in more realistic, seasonally varying
526 temperature regimes.

527 The temperature at which an epidemic started affected dynamics only under
528 large ranges of temperature variation. When temperature ranged from 10°C to 40°C,
529 the final epidemic size peaked at intermediate starting temperatures (24°C; Fig. 3,
530 A). However, in highly suitable seasonal environments, final epidemic size was large
531 regardless of the starting temperature (Fig. 3, B).

532 At mean starting temperatures, epidemic suitability was sensitive to the
533 interaction between annual temperature mean and seasonal variation. Under low
534 seasonal temperature variation, a narrow band of annual mean temperatures
535 (approximately 25-35°C) had the highest epidemic suitability (Figs. 4 & S2-S5).
536 Outside this band of temperature regimes, suitability diminishes rapidly. Larger
537 seasonal variation in temperature lowers the range of optimal annual mean
538 temperatures (i.e., suitability is high in cooler places with larger seasonal variation
539 in temperature; Fig. 4).

540 The relationship between epidemic suitability and the seasonal temperature
541 regime also depended on the temperature at the epidemic onset. Three distinct
542 relationships emerged (Figs. 5 & S6-S7). At intermediate annual mean temperatures
543 of ~25-35°C and low seasonal temperature variation (~0-10°C), epidemic suitability
544 is insensitive to starting temperature because temperature is suitable for
545 transmission year-round. At lower annual mean temperatures (~10-25°C) and
546 higher seasonal temperature variation (~10-15°C), epidemic suitability is highest
547 when epidemics start in moderate to warm seasons, and lower when epidemics

548 start during cooler seasons. Finally, at high annual mean temperatures ($> 35^{\circ}\text{C}$) and
549 low seasonal temperature variation ($\sim 0\text{-}10^{\circ}\text{C}$), epidemic suitability is high only
550 when epidemics start at the coldest period of the year, because otherwise the
551 temperature is too warm for efficient transmission. The interaction between
552 temperature mean, annual variation, and starting point sharply illustrates the
553 unimodal effect of temperature on transmission. Models that do not include
554 unimodal effects of temperature (e.g., those with sinusoidal forcing on a
555 transmission parameter) may fail to capture the limits on transmission in warm
556 environments.

557 With rising mean annual temperatures and increasing seasonal temperature
558 variation due to climate change, the landscape of epidemic suitability is likely to
559 shift. Importantly, areas with previously low epidemic suitability may have
560 increasing potential for transmission year-round. By contrast, warming
561 temperatures may drive epidemics in cities with high current suitability (e.g.,
562 Manila, Philippines, Barranquilla, Colombia, and Fortaleza, Brazil) to shift toward
563 cooler months. Thus, climate change may alter not only epidemic size and duration
564 but also seasonal timing globally, as it interacts with other important drivers like
565 rainfall and human behavior.

566 It is important to note that model-estimated epidemic suitability should be
567 treated as an upper bound on the potential for large epidemics because within
568 highly suitable climate regimes, epidemics can vary in magnitude due to human
569 population size and movement dynamics [28], effective vector control, and other

570 mitigating factors. Likewise, our estimates are conditioned on *Aedes aegypti*
571 presence and virus introduction to support an outbreak.

572 Although seasonal temperature dynamics provide insight into vector-borne
573 transmission dynamics, other factors like mosquito abundance, vector control, and
574 rainfall also determine transmission dynamics. Thus, temperature must be
575 considered jointly with these factors. Moreover, accurately describing epidemic
576 dynamics of emerging and established vector-borne pathogens will ultimately
577 require integrating realistic models of environmental suitability, as presented here,
578 with demographic, social, and economic factors that promote or limit disease
579 transmission [42,43]. Conversely, we show that the interaction between
580 temperature and the availability of susceptible hosts alone can drive epidemic
581 burnout even in the absence of other limiting factors like vector control and
582 seasonal precipitation. This suggests that correctly representing the nonlinear
583 relationship between temperature and epidemic dynamics is critical for accurately
584 inferring mechanistic drivers of epidemics and, in turn, predicting the efficacy of
585 control interventions.

586 References

- 587 1. Gubler DJ. The global emergence/resurgence of arboviral diseases as public
588 health problems. *Arch Med Res.* 2002;33: 330–342.
- 589 2. Faria NR, Azevedo R do S da S, Kraemer MUG, Souza R, Cunha MS, Hill SC, et
590 al. Zika virus in the Americas: Early epidemiological and genetic findings. *Science.*
591 2016;352: 345–349. doi:10.1126/science.aaf5036
- 592 3. Staples JE, Breiman RF, Powers AM. Chikungunya Fever: An Epidemiological
593 Review of a Re-Emerging Infectious Disease. *Clin Infect Dis.* 2009;49: 942–948.
594 doi:10.1086/605496
- 595 4. Special Programme for Research and Training in Tropical Diseases, World Health
596 Organization, editors. *Dengue: guidelines for diagnosis, treatment, prevention, and*
597 *control.* New ed. Geneva: TDR : World Health Organization; 2009.
- 598 5. Gubler DJ. Dengue/dengue haemorrhagic fever: history and current status.
599 *Novartis Found Symp.* 2006;277: 3–16; discussion 16-22, 71–73, 251–253.
- 600 6. Brady OJ, Gething PW, Bhatt S, Messina JP, Brownstein JS, Hoen AG, et al.
601 Refining the global spatial limits of dengue virus transmission by evidence-based
602 consensus. *PLoS Negl Trop Dis.* 2012;6: e1760. doi:10.1371/journal.pntd.0001760
- 603 7. Bhatt S, Gething PW, Brady OJ, Messina JP, Farlow AW, Moyes CL, et al. The
604 global distribution and burden of dengue. *Nature.* 2013;496: 504–507.
605 doi:10.1038/nature12060
- 606 8. Khan K, Bogoch I, Brownstein JS, Miniota J, Nicolucci A, Hu W, et al. Assessing
607 the origin of and potential for international spread of chikungunya virus from the
608 Caribbean. *PLoS Curr.* 2014;6.
609 doi:10.1371/currents.outbreaks.2134a0a7bf37fd8d388181539fea2da5
- 610 9. Perkins TA, Metcalf CJE, Grenfell BT, Tatem AJ. Estimating drivers of
611 autochthonous transmission of chikungunya virus in its invasion of the americas. *PLoS*
612 *Curr.* 2015;7. doi:10.1371/currents.outbreaks.a4c7b6ac10e0420b1788c9767946d1fc
- 613 10. Nsoesie EO, Kraemer MU, Golding N, Pigott DM, Brady OJ, Moyes CL, et al.
614 Global distribution and environmental suitability for chikungunya virus, 1952 to 2015.
615 *Euro Surveill Bull Eur Sur Mal Transm Eur Commun Dis Bull.* 2016;21.
616 doi:10.2807/1560-7917.ES.2016.21.20.30234
- 617 11. PAHO. Regional Zika Epidemiological Update (Americas) August 25, 2017. Pan
618 American Health Organization;
- 619 12. Bjornstad ON, Finkenstadt BF, Grenfell BT. Dynamics of Measles Epidemics:
620 Estimating Scaling of Transmission Rates Using a Time Series SIR Model. *Ecol Monogr.*
621 2002;72: 169. doi:10.2307/3100023
- 622 13. Coburn BJ, Wagner BG, Blower S. Modeling influenza epidemics and
623 pandemics: insights into the future of swine flu (H1N1). *BMC Med.* 2009;7.
624 doi:10.1186/1741-7015-7-30
- 625 14. Kucharski AJ, Funk S, Eggo RM, Mallet H-P, Edmunds WJ, Nilles EJ.
626 Transmission Dynamics of Zika Virus in Island Populations: A Modelling Analysis of the
627 2013–14 French Polynesia Outbreak. Barker CM, editor. *PLoS Negl Trop Dis.* 2016;10:
628 e0004726. doi:10.1371/journal.pntd.0004726
- 629 15. Eisen L, Monaghan AJ, Lozano-Fuentes S, Steinhoff DF, Hayden MH, Bieringer
630 PE. The impact of temperature on the bionomics of *Aedes (Stegomyia) aegypti*, with

- 631 special reference to the cool geographic range margins. *J Med Entomol.* 2014;51: 496–
632 516.
- 633 16. Rueda LM, Patel KJ, Axtell RC, Stinner RE. Temperature-dependent
634 development and survival rates of *Culex quinquefasciatus* and *Aedes aegypti* (Diptera:
635 Culicidae). *J Med Entomol.* 1990;27: 892–898.
- 636 17. Tun-Lin W, Burkot TR, Kay BH. Effects of temperature and larval diet on
637 development rates and survival of the dengue vector *Aedes aegypti* in north Queensland,
638 Australia. *Med Vet Entomol.* 2000;14: 31–37.
- 639 18. Kamimura K, Matsuse IT, Takahashi H, Komukai J, Fukuda T, Suzuki K, et al.
640 Effect of temperature on the development of *Aedes aegypti* and *Aedes albopictus*. *Med*
641 *Entomol Zool.* 2002;53: 53–58. doi:10.7601/mez.53.53_1
- 642 19. Beserra EB, Fernandes CRM, Silva SA de O, Silva LA da, Santos JW dos. Efeitos
643 da temperatura no ciclo de vida, exigências térmicas e estimativas do número de gerações
644 anuais de *Aedes aegypti* (Diptera, Culicidae). *Iheringia Sér Zool.* 2009;99: 142–148.
645 doi:10.1590/S0073-47212009000200004
- 646 20. Couret J, Dotson E, Benedict MQ. Temperature, larval diet, and density effects on
647 development rate and survival of *Aedes aegypti* (Diptera: Culicidae). *PloS One.* 2014;9:
648 e87468. doi:10.1371/journal.pone.0087468
- 649 21. Watts DM, Burke DS, Harrison BA, Whitmire RE, Nisalak A. Effect of
650 temperature on the vector efficiency of *Aedes aegypti* for dengue 2 virus. *Am J Trop Med*
651 *Hyg.* 1987;36: 143–152.
- 652 22. McLean DM, Clarke AM, Coleman JC, Montalbetti CA, Skidmore AG, Walters
653 TE, et al. Vector capability of *Aedes aegypti* mosquitoes for California encephalitis and
654 dengue viruses at various temperatures. *Can J Microbiol.* 1974;20: 255–262.
- 655 23. Altizer S, Dobson A, Hosseini P, Hudson P, Pascual M, Rohani P. Seasonality
656 and the dynamics of infectious diseases. *Ecol Lett.* 2006;9: 467–484. doi:10.1111/j.1461-
657 0248.2005.00879.x
- 658 24. Mordecai EA, Cohen JM, Evans MV, Gudapati P, Johnson LR, Lippi CA, et al.
659 Detecting the impact of temperature on transmission of Zika, dengue, and chikungunya
660 using mechanistic models. *PLoS Negl Trop Dis.* 2017;11: e0005568.
661 doi:10.1371/journal.pntd.0005568
- 662 25. Yang HM, Macoris MLG, Galvani KC, Andrighetti MTM, Wanderley DMV.
663 Assessing the effects of temperature on dengue transmission. *Epidemiol Infect.* 2009;137:
664 1179–1187. doi:10.1017/S0950268809002052
- 665 26. Yang HM, Boldrini JL, Fassoni AC, Freitas LFS, Gomez MC, de Lima KKB, et
666 al. Fitting the Incidence Data from the City of Campinas, Brazil, Based on Dengue
667 Transmission Modellings Considering Time-Dependent Entomological Parameters. *PloS*
668 *One.* 2016;11: e0152186. doi:10.1371/journal.pone.0152186
- 669 27. Johansson MA, Powers AM, Pesik N, Cohen NJ, Staples JE. Nowcasting the
670 spread of chikungunya virus in the Americas. *PloS One.* 2014;9: e104915.
671 doi:10.1371/journal.pone.0104915
- 672 28. Wesolowski A, Qureshi T, Boni MF, Sundsøy PR, Johansson MA, Rasheed SB,
673 et al. Impact of human mobility on the emergence of dengue epidemics in Pakistan. *Proc*
674 *Natl Acad Sci U S A.* 2015;112: 11887–11892. doi:10.1073/pnas.1504964112
- 675 29. Liu-Helmersson J, Stenlund H, Wilder-Smith A, Rocklöv J. Vectorial capacity of
676 *Aedes aegypti*: effects of temperature and implications for global dengue epidemic

- 677 potential. *PloS One*. 2014;9: e89783. doi:10.1371/journal.pone.0089783
- 678 30. Morin CW, Monaghan AJ, Hayden MH, Barrera R, Ernst K. Meteorologically
679 Driven Simulations of Dengue Epidemics in San Juan, PR. *PLoS Negl Trop Dis*. 2015;9:
680 e0004002. doi:10.1371/journal.pntd.0004002
- 681 31. Caminade C, Turner J, Metelmann S, Hesson JC, Blagrove MSC, Solomon T, et
682 al. Global risk model for vector-borne transmission of Zika virus reveals the role of El
683 Niño 2015. *Proc Natl Acad Sci U S A*. 2017;114: 119–124.
684 doi:10.1073/pnas.1614303114
- 685 32. Lourenço J, Recker M. The 2012 Madeira dengue outbreak: epidemiological
686 determinants and future epidemic potential. *PLoS Negl Trop Dis*. 2014;8: e3083.
687 doi:10.1371/journal.pntd.0003083
- 688 33. Faria NR, da Costa AC, Lourenço J, Loureiro P, Lopes ME, Ribeiro R, et al.
689 Genomic and epidemiological characterisation of a dengue virus outbreak among blood
690 donors in Brazil. *Sci Rep*. 2017;7: 15216. doi:10.1038/s41598-017-15152-8
- 691 34. Lourenço J, Maia de Lima M, Faria NR, Walker A, Kraemer MU, Villabona-
692 Arenas CJ, et al. Epidemiological and ecological determinants of Zika virus transmission
693 in an urban setting. *eLife*. 2017;6. doi:10.7554/eLife.29820
- 694 35. Duong V, Lambrechts L, Paul RE, Ly S, Lay RS, Long KC, et al. Asymptomatic
695 humans transmit dengue virus to mosquitoes. *Proc Natl Acad Sci U S A*. 2015;112:
696 14688–14693. doi:10.1073/pnas.1508114112
- 697 36. Appassakij H, Khuntikij P, Kemapunmanus M, Wutthanarungsan R, Silpapojakul
698 K. Viremic profiles in asymptomatic and symptomatic chikungunya fever: a blood
699 transfusion threat? *Transfusion (Paris)*. 2013;53: 2567–2574. doi:10.1111/j.1537-
700 2995.2012.03960.x
- 701 37. Murphy BR, Whitehead SS. Immune response to dengue virus and prospects for a
702 vaccine. *Annu Rev Immunol*. 2011;29: 587–619. doi:10.1146/annurev-immunol-031210-
703 101315
- 704 38. Weaver SC, Osorio JE, Livengood JA, Chen R, Stinchcomb DT. Chikungunya
705 virus and prospects for a vaccine. *Expert Rev Vaccines*. 2012;11: 1087–1101.
706 doi:10.1586/erv.12.84
- 707 39. Le Menach A, McKenzie FE, Flahault A, Smith DL. The unexpected importance
708 of mosquito oviposition behaviour for malaria: non-productive larval habitats can be
709 sources for malaria transmission. *Malar J*. 2005;4: 23. doi:10.1186/1475-2875-4-23
- 710 40. Palamara GM, Childs DZ, Clements CF, Petchey OL, Plebani M, Smith MJ.
711 Inferring the temperature dependence of population parameters: the effects of
712 experimental design and inference algorithm. *Ecol Evol*. 2014;4: 4736–4750.
713 doi:10.1002/ece3.1309
- 714 41. Perkins TA. Retracing Zika's footsteps across the Americas with computational
715 modeling. *Proc Natl Acad Sci U S A*. 2017;114: 5558–5560.
716 doi:10.1073/pnas.1705969114
- 717 42. Zhang Q, Sun K, Chinazzi M, Pastore Y Piontti A, Dean NE, Rojas DP, et al.
718 Spread of Zika virus in the Americas. *Proc Natl Acad Sci U S A*. 2017;114: E4334–
719 E4343. doi:10.1073/pnas.1620161114
- 720 43. Alex Perkins T, Siraj AS, Ruktanonchai CW, Kraemer MUG, Tatem AJ. Model-
721 based projections of Zika virus infections in childbearing women in the Americas. *Nat*
722 *Microbiol*. 2016;1: 16126. doi:10.1038/nmicrobiol.2016.126

723

724 **Supporting Information Legends**

725 **S1 Fig. Sensitivity of epidemiological indices as a function of starting**

726 **temperature to the parametrization of life history traits.** The red curve

727 represents the median maximum number of humans in the infected class (I_H) at any

728 given point during the simulation. The blue curve represents the median final (or

729 cumulative) epidemic size (R_H at the final time step). The green curve represents the

730 median length of the epidemic (i.e., the point at which the number of infected

731 individuals was below one). Each shaded area represents the 95% credible interval

732 for the epidemiological indices ran under 50 different parameterizations of the life

733 history traits. Here, simulations were run with the temperature conditions: $T_{min} =$

734 10°C , $T_{mean} = 25^\circ\text{C}$, and $T_{max} = 40^\circ\text{C}$ (A) and $T_{min} = 20^\circ\text{C}$, $T_{mean} = 25^\circ\text{C}$, and $T_{max} = 30^\circ\text{C}$

735 (B).

736 **S2 Fig. Variation in epidemic suitability across different seasonal temperature**

737 **regimes with 20% population immunity.** The heat map shows the epidemic

738 suitability (represented as the proportion of the total human population infected

739 during an epidemic) as a function of mean annual temperature and temperature

740 range assuming 20% population immunity. Here, temperature range is defined as

741 the seasonal variation about the annual mean temperature. Twenty large, globally

742 important cities are plotted to illustrate their epidemic suitability.

743 **S3 Fig. Variation in epidemic suitability across different seasonal temperature**

744 **regimes with 40% population immunity.** The heat map shows the epidemic

745 suitability (represented as the proportion of the total human population infected

746 during an epidemic) as a function of mean annual temperature and temperature

747 range assuming 40% population immunity. Here, temperature range is defined as
748 the seasonal variation about the annual mean temperature. Twenty large, globally
749 important cities are plotted to illustrate their epidemic suitability.

750 **S4 Fig. Variation in epidemic suitability across different seasonal temperature**

751 **regimes with 60% population immunity.** The heat map shows the epidemic
752 suitability (represented as the proportion of the total human population infected
753 during an epidemic) as a function of mean annual temperature and temperature
754 range assuming 60% population immunity. Here, temperature range is defined as
755 the seasonal variation about the annual mean temperature. Twenty large, globally
756 important cities are plotted to illustrate their epidemic suitability.

757 **S5 Fig. Variation in epidemic suitability across different seasonal temperature**

758 **regimes with 80% population immunity.** The heat map shows the epidemic
759 suitability (represented as the proportion of the total human population infected
760 during an epidemic) as a function of mean annual temperature and temperature
761 range assuming 80% population immunity. Here, temperature range is defined as
762 the seasonal variation about the annual mean temperature. Twenty large, globally
763 important cities are plotted to illustrate their epidemic suitability.

764 **S6 Fig. Variation in epidemic suitability across different seasonal temperature**

765 **regimes with minimum starting temperature.** The heat map shows the epidemic
766 suitability (represented as the proportion of the total human population infected
767 during an epidemic) as a function of mean annual temperature and temperature
768 range. Here, temperature range is defined as the seasonal variation about the annual
769 mean temperature, and the simulation began at the minimum temperature of the

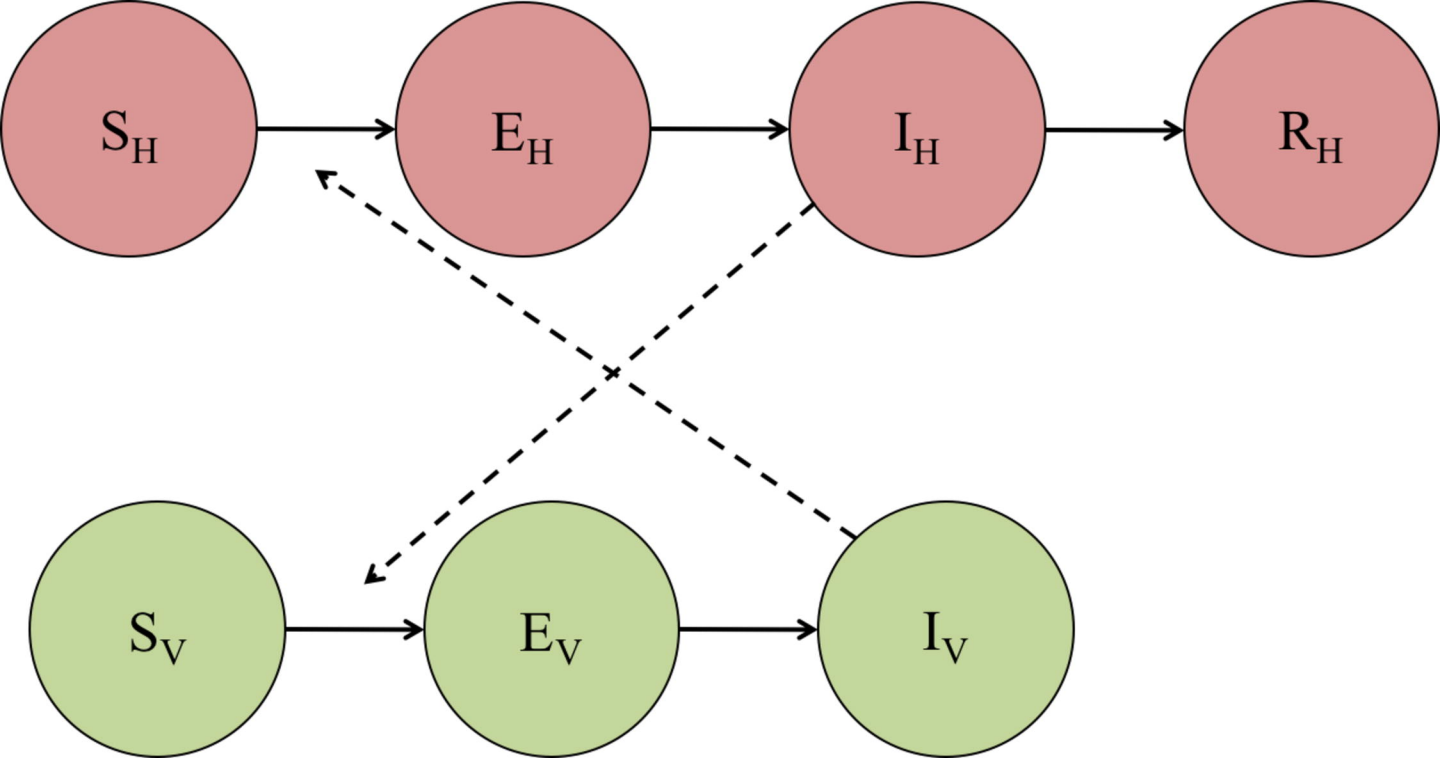
770 regime. Twenty large, globally important cities are plotted to illustrate their
771 epidemic suitability.

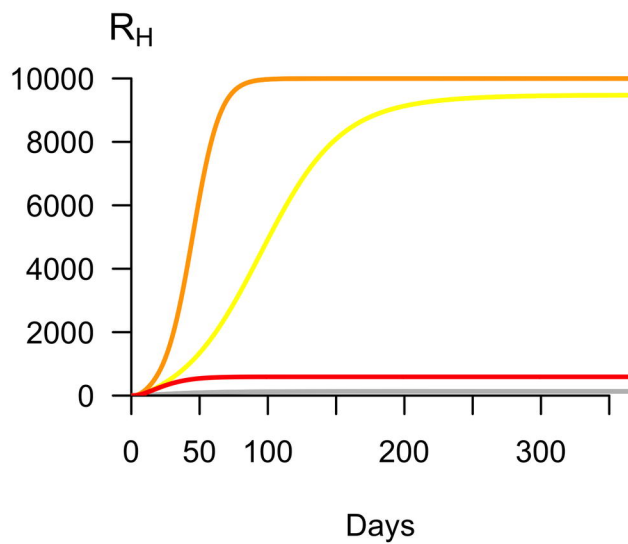
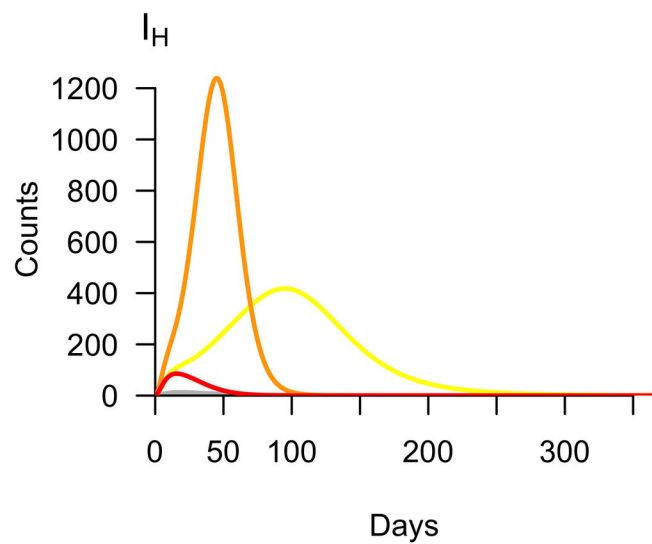
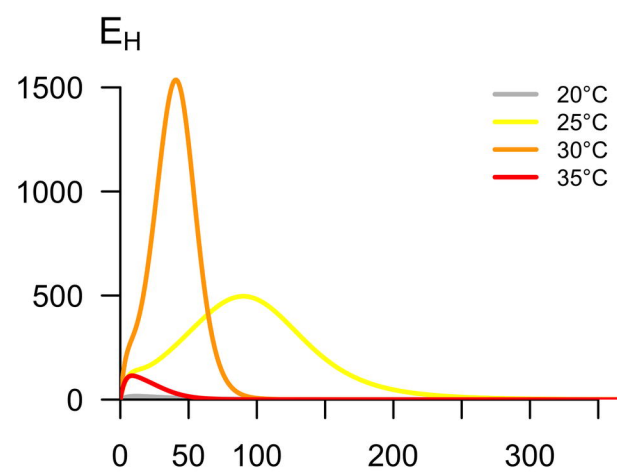
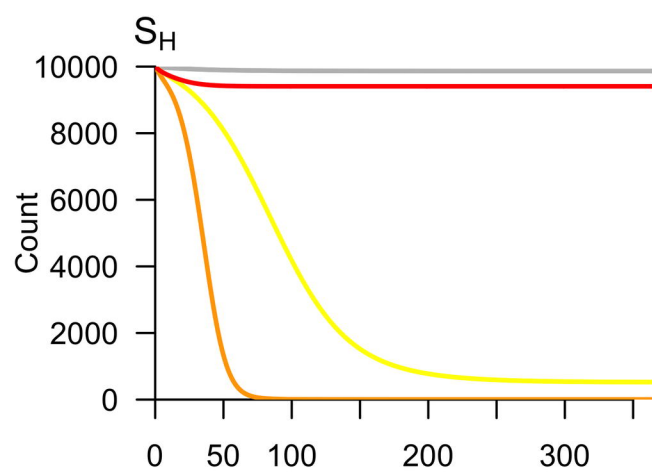
772 **S7 Fig. Variation in epidemic suitability across different seasonal temperature**
773 **regimes with maximum starting temperature.** The heat map shows the epidemic
774 suitability (represented as the proportion of the total human population infected
775 during an epidemic) as a function of mean annual temperature and temperature
776 range. Here, temperature range is defined as the seasonal variation about the annual
777 mean temperature, and the simulation began at the maximum temperature of the
778 regime. Twenty large, globally important cities are plotted to illustrate their
779 epidemic suitability.

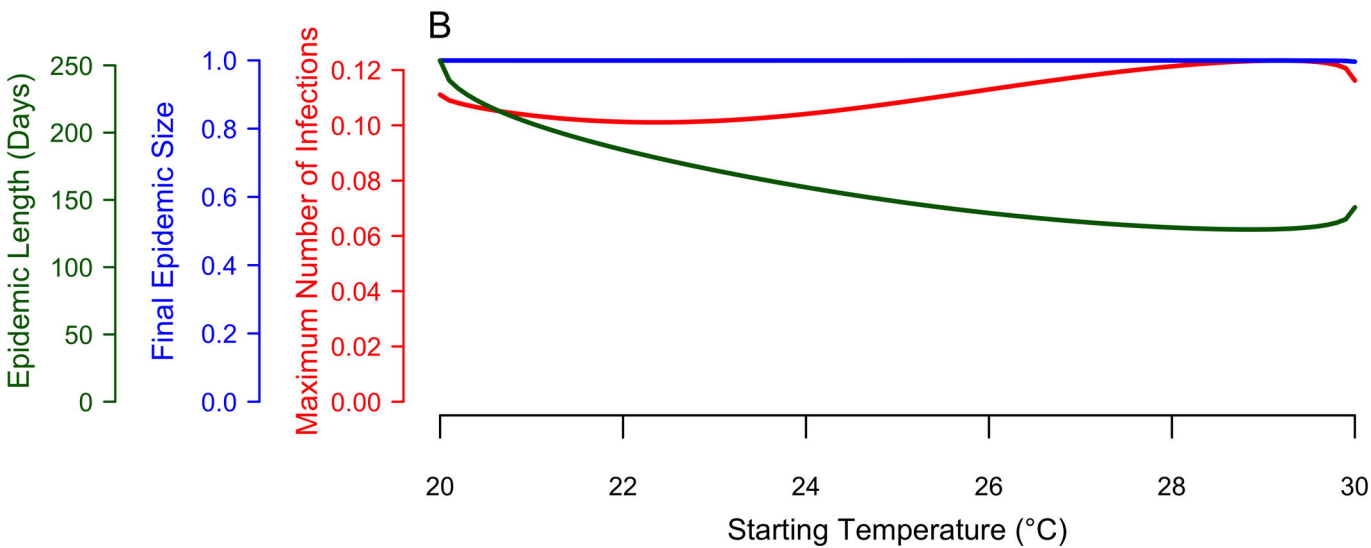
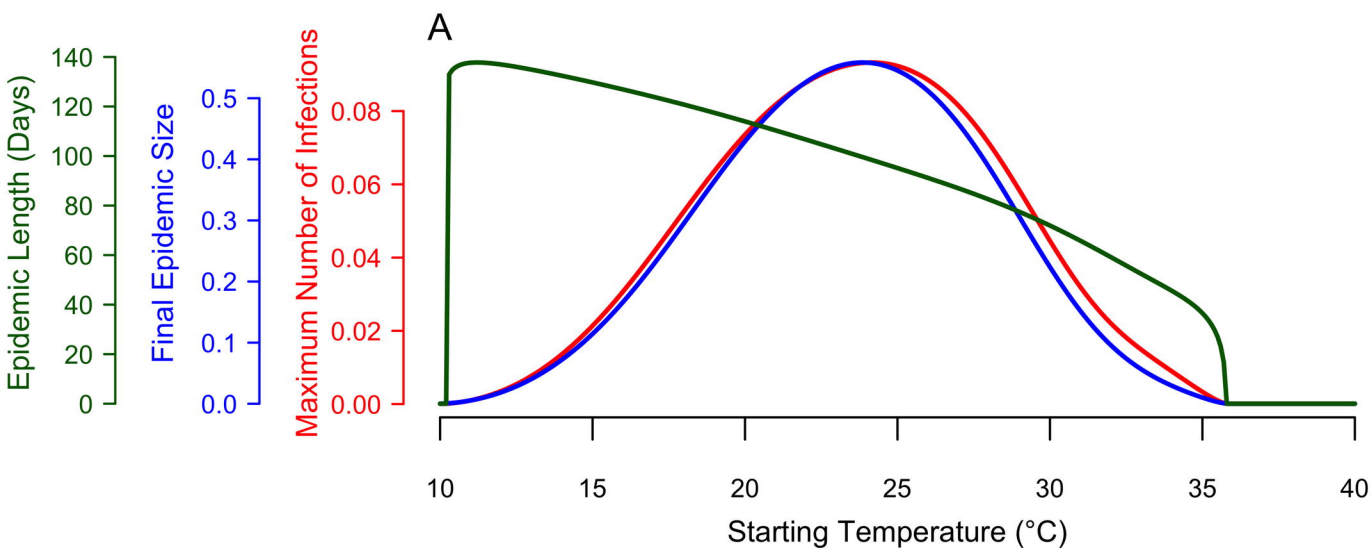
780 **S8 Fig. The 2.5% quantile of epidemic suitability to the parameterization of**
781 **life history traits.** Epidemic suitability (represented as the proportion of the total
782 human population infected during an epidemic) as a function of mean annual
783 temperature and the temperature range. Temperature varied according to a
784 seasonal temperature regime, and 50 samples of c , T_{\min} , and T_{\max} were taken from
785 the joint posterior distribution of each trait thermal response from Mordecai et al.
786 [24].

787 **S9 Fig. The 50% quantile of epidemic suitability to the parameterization of life**
788 **history traits.** Epidemic suitability (represented as the proportion of the total
789 human population infected during an epidemic) as mean annual temperature and
790 the temperature range. Temperature varied according to a seasonal temperature
791 regime, and 50 samples of c , T_{\min} , and T_{\max} were taken from the joint posterior
792 distribution of each trait thermal response from Mordecai et al. [24].

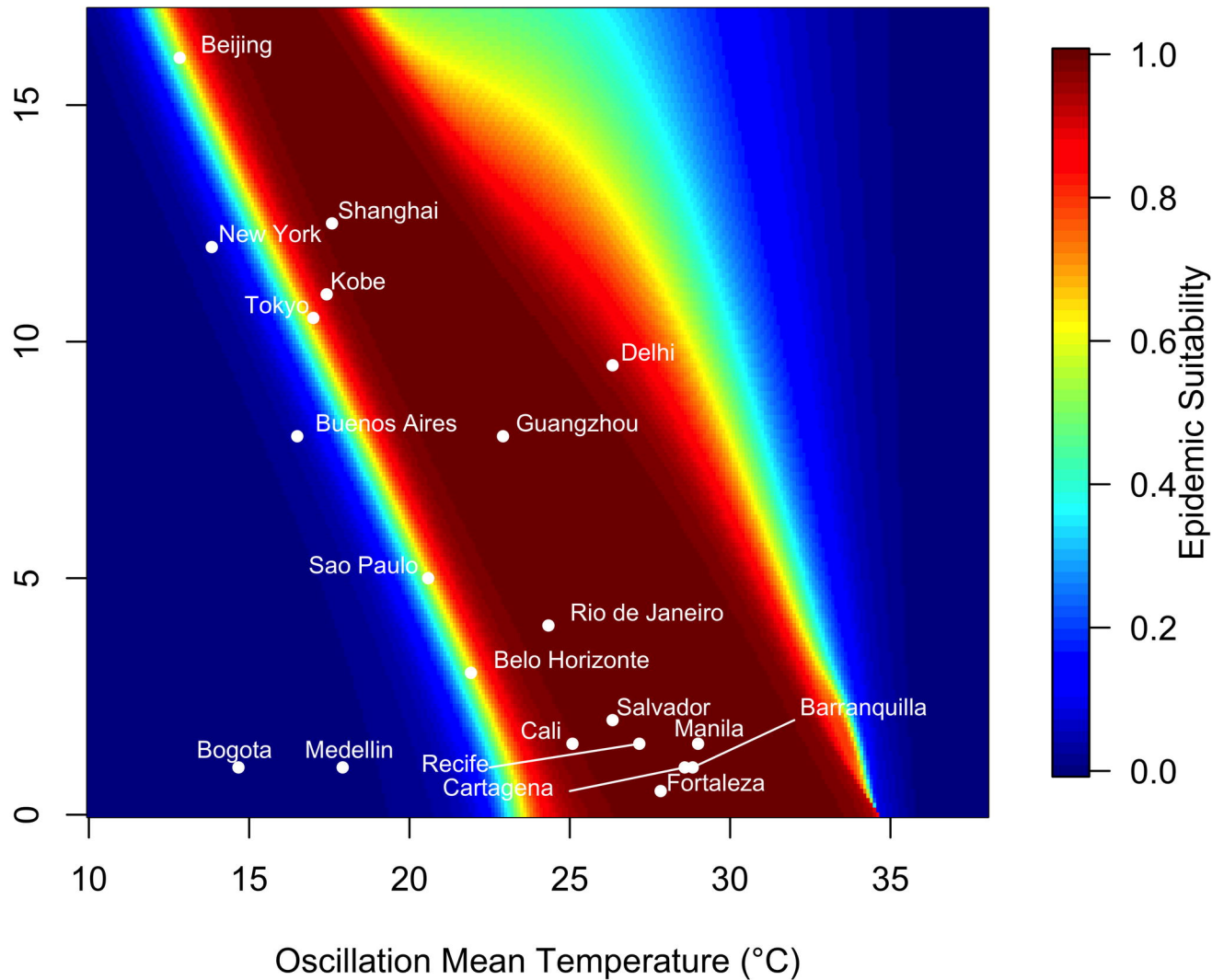
793 **S10 Fig. The 97.5% quantile of epidemic suitability to the parameterization of**
794 **life history traits.** Epidemic suitability (represented as the proportion of the total
795 human population infected during an epidemic) as mean annual temperature and
796 the temperature range. Temperature varied according to a seasonal temperature
797 regime, and 50 samples of c , T_{\min} , and T_{\max} were taken from the joint posterior
798 distribution of each trait thermal response from Mordecai et al. [24].
799
800







Amplitude (°C)



Amplitude (°C)

